

Organic photovoltaics

In the last ten years, the highest efficiency obtained from organic photovoltaics (OPVs), such as bulk heterojunction polymer:fullerene solar cells, has risen from 2.5 to 11 %. This rapid progress suggests that the commercialization of OPVs should be realized soon if we can solve some technical issues. The advances in the development of OPVs can be attributed to four fronts: (i) a better understanding of the mechanism of photon-to-electron conversion; (ii) new materials with tailored energy levels and solubility; (iii) new processing approaches to induce optimal microstructures in the active layer; and (iv) new device architectures with novel interfacial layers. Herein, we review the materials, the microstructures of the active layers, the device structures, the interfacial layers that have been developed recently for OPVs, and provide future perspectives for this promising technology.

Yu-Wei Su, Shang-Che Lan, and Kung-Hwa Wei*

Department of Materials Science and Engineering, National Chiao Tung University, Hsinchu 30049, Taiwan

**E-mail: khwei@mail.nctu.edu.tw*

The field of organic photovoltaics (OPVs) has progressed quite significantly in the last ten years, not only for their academic interest but also for their potential as an affordable energy technology, with high-throughput roll-to-roll solution processing driving down costs to the point of competitiveness with current technologies. Moreover, OPVs are light, can have tandem structures, and can be fabricated on plastic substrates, with flexibility to conform to the human body for potential applications in consumer electronics. Because OPVs can also be transparent or color-tunable, they can be integrated into building components for a variety of applications. Fig. 1 displays the evolution of the record efficiencies of single- and multi-junction

organic solar cells; at present, the highest efficiency is near 11 %¹. Despite the advantages of and progress in the development of OPVs, several technical hurdles must be overcome prior to the successful launch of this promising technology to the market. In this review, we focus our attention mostly on polymer photovoltaics and some small molecule photovoltaics due to limited space. We discuss the basic mechanism for device operation; the relationship between material properties and power conversion efficiency (PCE); the molecular engineering of polymers and fullerenes; the microstructure of the active layer; the device structure and interfacial layers; and conclude with future perspectives.

Mechanism of photon-to-electron conversion process

Fig. 2 illustrates the four fundamental steps involved in the photon-to-electron conversion mechanism for OPVs. First, upon the absorption of light, an electron in the donor undergoes photoinduced excitation from the highest occupied molecular orbital (HOMO) to the lowest unoccupied molecular orbital (LUMO) of the organic material, forming a Frenkel exciton (coulombically bound electron (e^-) and hole (h^+)). The ratio of the generated Frenkel excitons to the total incident photons, in terms of energy, is defined as the absorption efficiency (η_A). Excitons in organic materials have a binding energy² of 0.5–1 eV, due to their low dielectric permittivity³ ($\epsilon = 3 - 4$). In comparison, thermal energy (kT) at a room temperature (298 K) is approximately 0.025 eV, substantially lower than the binding energy (0.5–1 eV) of an exciton in an organic material. Thus, if the organic material is to serve as an electron donor in OPVs, a second material is required as an electron acceptor to ensure a built-in internal field at the interface to break up any excitons that diffuse there into free carriers. The most widely used acceptor materials are fullerenes, which have electron affinities greater than those of polymers or small molecules.

Second, the excitons must diffuse to the donor–acceptor (D–A) interfaces within the diffusion length (L_D) to prevent recombining to the ground state. Because the value of L_D in organic materials⁴ is typically 10 nm, the ideal donor or acceptor domain size is less than 20 nm. This D–A interface concept is analogous—in terms of charge transport—to a P–N junction in an inorganic semiconductor. The ratio of the number of excitons that reach the D–A interface to the total number of excitons generated through photoexcitation is defined as the exciton diffusion efficiency (η_{ED}).

Third, an exciton at a D–A interface undergoes charge-transfer (CT) process at an ultrafast pace⁵ (ca. 100 fs) to form a CT exciton, where the hole and electron remain in the donor and acceptor phases, respectively, held together through coulombic attraction. The charge separation efficiency (η_{CS}) is defined as the ratio of the number of excitons that have undergone the CT process to the number of excitons that have reached the D–A interface. Fourth, the CT exciton dissociates, as a result of the built-in electric field, into free holes and electrons, which are then transported through the donor and acceptor phases, respectively, to their respective electrodes. The transport of free carriers to the respective electrodes occurs within a period of time ranging from nano- to microseconds. The charge collection efficiency (η_{CC}) is defined as the ratio of the number of carriers that have been collected at the electrodes to the number of excitons that have undergone the CT process. Two recent developments in this area have been (i) it is possible for every absorbed photon resulting in a separated pair of charge carriers and all photogenerated carriers being collected at the electrode for a push-pull polymer⁶ when an TiOx optical spacer was incorporated in the device and (ii) when polymer and fullerenes are mixed at the molecular level, photogenerated excitons are next to the heterojunction and often do not need to diffuse to the interfaces⁷ for CT process

Relationship between the energy band and the PCE of a device

For a photon-to-electron conversion process, the external quantum efficiency (EQE) is defined as the ratio between the collected photo-

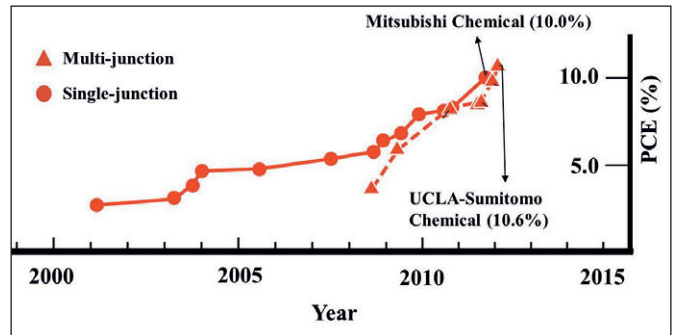


Fig. 1 Evolution of the record efficiencies of single- and multi-junction polymer solar cells. Reprinted with permission from Ref1. Copyright © National Renewable Energy Laboratory.

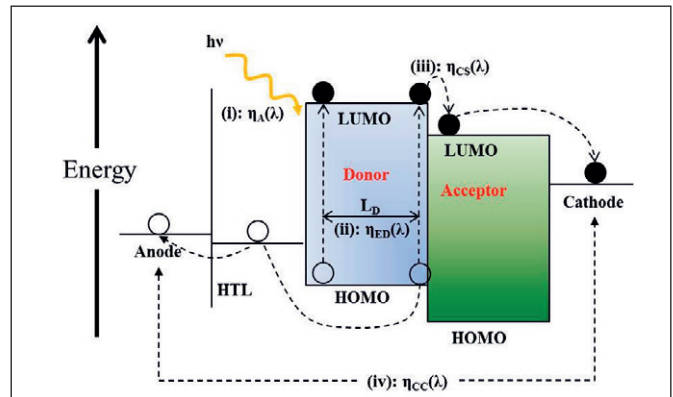


Fig. 2 Fundamental mechanism of the photon-to-electron conversion process in bulk heterojunction solar cells.

generated charges at the electrodes to the number of incident photons at a particular wavelength (i.e., EQE is a function of wavelength), in terms of energy. The EQE can be expressed in equation (1).

$$\text{EQE}(\lambda) = \eta_A(\lambda) \times \eta_{ED}(\lambda) \times \eta_{CS}(\lambda) \times \eta_{CC}(\lambda) \quad (1)$$

where λ is the wavelength of incident light. The PCE, $\eta(\%)$, of a photovoltaic device is defined by the equation (2)

$$\eta = (J_{sc} \times V_{oc} \times FF) / P_{in} \quad (2)$$

where J_{sc} , V_{oc} , FF, and P_{in} are the short-circuit current density, open-circuit voltage, fill factor, and power of incident light, respectively. The value of J_{sc} is influenced by the breadth of the light absorption spectrum (determined mainly by the bandgap), the extent of light absorption (determined by the thickness of the active layer), and the morphology of the active layer. Theoretically, the J_{sc} is defined by equation (3).

$$J_{sc} = \frac{hc}{q} \int \frac{P_{sun}(\lambda) \cdot \text{EQE}(\lambda)}{\lambda} d\lambda \quad (3)$$

where P_{sun} represents the solar spectrum, q the elementary charge, h the Planck constant, and c the speed of light. The open-circuit voltage,

V_{oc} is the maximum potential at which there is no current. Theoretically, the value of V_{oc} is linearly proportional to the difference in energy levels between the HOMO of the donor and the LUMO of the acceptor. Therefore, to enlarge the value of V_{oc} , one can either lower the HOMO of the donor or raise the LUMO of the acceptor. For effective CT process, however, the LUMO of the conjugated polymer must be higher⁸ (by at least 0.3 eV) than that of the fullerene. Hence, the value of V_{oc} is determined essentially by the material properties of the donor and acceptor in the active layer, although different cathode materials also have an effect. The FF is sensitive to competition between photocurrent generation and charge recombination and therefore is significantly impacted by the morphology of the active layer.

The light absorption saturation thickness for a polymeric material is ca. 200 nm (180 μm for silicon), differing greatly from the exciton diffusion length. It indicates that applying a bilayer (donor layer/acceptor) heterojunction is not an ideal structure for OPVs. Instead, the concept of a bulk heterojunction (BHJ) structure, in which a conjugated polymer donor is intimately blended with a fullerene derivative (dimensions: ca. 1–2 nm), was conceived for the active layer⁹. BHJ-structured active layer that provides many localized D–A interfaces for charge separation is the most successful structure for OPVs. These fullerene moieties tend to form aggregated domains as a result of π – π electron attraction; so does the polymer, if it possesses suitable crystallinity. These donor and acceptor phase domains in the active layer provide not only interfaces for charge separation of the photogenerated excitons but also percolation pathways for charge transport to the respective electrodes, affecting the value of J_{sc} critically. The ideal active layer morphology would feature an interpenetrating D–A network with either the donor or acceptor domains having significantly optimal dimensions that are less than the exciton diffusion length. In actual cases, hierarchical structures have been found in the active layer where molecularly-mixed polymer:fullerene amorphous domains coexist with phase-separated polymer and fullerene domains. The thickness of the active layer is a compromise because a thicker layer tends to absorb more light, but raises the possibility of charge recombination in the longer paths to the respective electrodes; the optimal thickness of the active layer is, therefore, between 100 and 150 nm (the active layer can be thicker for crystalline organic materials or when continuous percolating networks are present).

Molecular engineering of push/pull conjugated polymers for energy band and solubility tuning

For conjugated polymers or small molecules to be used in OPVs, they would ideally exhibit (i) low bandgaps to broaden the absorption range; (ii) crystalline characteristics to ensure good charge mobility; (iii) low HOMO energy levels to enhance the values of V_{oc} ; and (iv) suitable LUMO energy levels for efficient electron transfer to the fullerene moieties. The relatively low values of J_{sc} found for OPVs arise mainly from the larger optical gaps of the organic molecules used, typically 1.5–2 eV (cf. 1.1 eV for silicon)¹⁰. Therefore, there is a need for low bandgap organic semiconductors with light absorption that extends further into the infrared (IR; i.e., to lower the bandgap). The architecture of the conjugated polymer is described by three basic units: its backbone repeating units, side

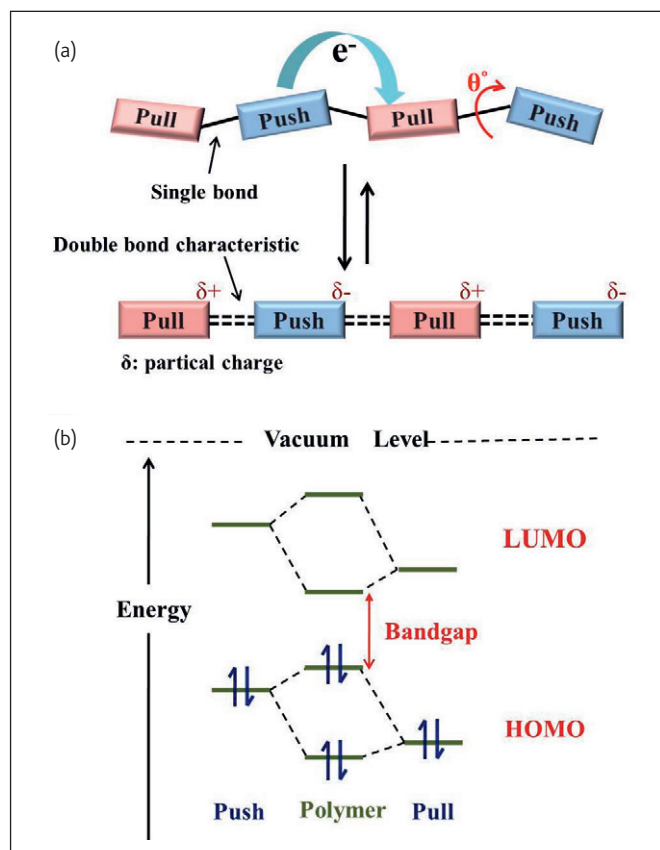


Fig 3. (a) the delocalization of π electrons and (b) the energy bands of push and pull units and the bandgap of a push/pull polymer.

chains, and substituents¹¹. The backbone repeating units, which consist of conjugated chains, generally determine the HOMO and LUMO energy levels and also the bandgap of the polymer (the molecular weight also affects the bandgap when it is less than 10 000 Da). The most successful strategy for harvesting more photons through tuning of the energy levels of conjugated polymers involves the incorporation of electron push/pull molecular units in the conjugated main chain. Alternating push and pull units that allow internal charge transfer process along the conjugated chain increase the effective resonance length of the π electrons, leading to smaller bandgaps as a result of facilitated π electron delocalization (i.e., through planarization)¹². Fig. 3 shows the delocalization of π electrons and the energy bands of push and pull units and the bandgap of a push/pull polymer.

Planarization may also decrease the optical gap further by enabling π -stacked aggregates to form. Through careful design and selection of the push and pull molecular units, we can tune the HOMO and LUMO energy levels—and, therefore, the bandgap—of a synthesized conjugated polymer, because its HOMO and LUMO energy levels are largely localized on the push and pull moieties, respectively¹³. Hence, a weakly electron-donating unit conjugated to a strongly electron-withdrawing unit is necessary to simultaneously decrease the HOMO energy level and the bandgap of a push/pull polymer and therefore to increase the V_{oc} and J_{sc} of the device simultaneously when blending the polymer with fullerenes. In addition,

the side chains and substituent atoms of a conjugated polymer can affect its solubility, molecular organization, and energy bands^{14,15}.

One of the most effective push units with a planar structure is the weak push unit benzo[1,2-*b*:4,5-*b'*]dithiophene (**BDT**). Members of a series of push/pull polymers incorporating **BDT** units, displaying low bandgaps ($E_g < 1.8$ eV) and low HOMO energy levels, have resulted in photovoltaic devices with high PCEs of 5 to 7 %¹⁶⁻¹⁸. When **BDT** units were copolymerized with the strong pull units of thieno[3,4-*b*]thiophene (**TT**) and benzo[2,1,3]thiadazole (**BT**) to form the push/pull polymers **PBDTTT**¹⁹ and **PBnDT-DTBT**²⁰ respectively, the devices made by these polymers blended with PC₇₁BM provided PCE greater than 5 %. Substituting a hydrogen atom on the thiophene or phenyl ring of a pull unit with a highly electronegative fluorine atom leads to dramatic decreases in both the LUMO and HOMO energy levels of the polymers. The PCEs of the devices, **PBDTTT**:PC₇₁BM and **PBnDT-DTBT**:PC₇₁BM, were enhanced to 7.7 and 7.3 %, respectively. All of the active layers described above were processed with an additive, 1,8-diiodooctane (DIO), to obtain optimal microstructures. Recently, another strong pull unit, thieno[3,4-*c*]pyrrole-4,6-dione (**TPD**), has been used in the design of push/pull polymers exhibiting high crystallinity and deep HOMO energy levels²¹⁻²³ that impart high hole mobilities and large values of V_{oc} . The symmetrical push units dithienosilole (**DTS**), dithienogermole (**DTGe**), and bithiophene (**BTh**) have been used to form conjugated structures with **TPD**, respectively resulting in the polymers **PDTSTPD**²⁴, **PDTGeTPD**²⁵, and **PBTTPD**^{26,27}, that have provided PCE greater than 7 % after blending with PC₇₁BM and processing with additives. Recently, **PDTGeTPD**:PC₇₁BM based inverted devices²⁸ that incorporated UV-Ozone treated ZnO-polyvinyl pyrrolidone layer have displayed a PCE of 8.5 %. Fluorinated **PBDTTT**:PC₇₁BM based inverted devices²⁹ that incorporate amino-group attached polyfluorene as the electron transport layer provided a PCE of 9.2 %. Up to now, the highest PCE for a single-junction cell is provided by Mitsubishi Chemical with a record of 10 % that has been certified by National Renewable Energy Laboratories (NREL), but no detail information on either the active layer composition or the device structure was given¹.

Another configuration of the push/pull architecture features a push unit in the main chain in conjugation with a pull unit in the side chain, thereby enhancing exciton dissociation and subsequent CT process to the fullerene moieties. This configuration results in a hole in the main chain and an electron in the side chain³⁰⁻³³. In addition, rational design of the side chain moieties can be used to fine-tune the energy gap and level of the polymer. For small molecules, the greatest challenge is the difficulty on forming spin-coated thin films, even though their structures are well controlled in every batch. A pull-push-pull small molecule, oligothiophene with cyanoacetate derivative³⁴, along with PC₆₁BM has been solution-processed to make a BHJ device with a PCE of 5.8 %. Additionally, a new small molecule thiophene and thiadiazolo derivative³⁵ was solution-processed with PC₇₁BM along with DIO to form a BHJ OPV having an efficiency of 6.7 %.

Molecular engineering of functionalized fullerene for energy band and solubility tuning

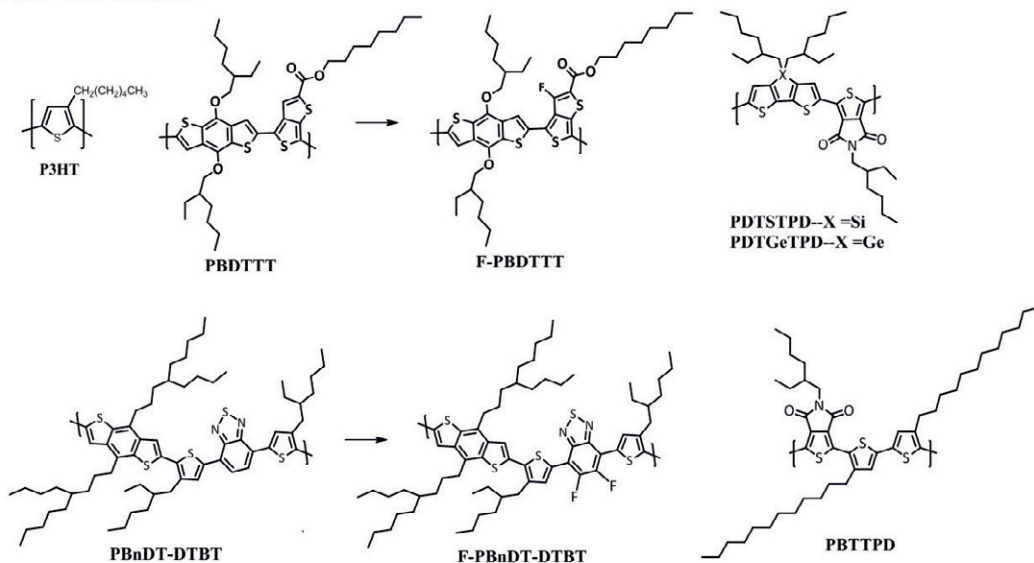
The development of acceptor materials has experienced relatively slow progress. Fullerene derivatives, such as PC₆₁BM and PC₇₁BM, not only

possess strong electron affinity but also exhibit good solubility and can be self-assembled into appropriate domains in the active layer. PC₆₁BM exhibits weak absorption because of symmetry-forbidden optical transitions; although PC₇₁BM absorbs between 400 and 530 nm, it can display some dispersion issues in polymers, often requiring the use of additives to decrease the size of the PC₇₁BM grain boundaries. Alternative fullerenes featuring higher LUMO energy levels, such as bis-PC₆₁BM³⁶, tris-PC₆₁BM³⁷, and indene-fullerene bisadduct (ICBA)³⁸⁻⁴⁰, have also been blended with polymers to enhance the values of V_{oc} of the devices. Fig. 4 shows the chemical structures of representative donors (polymers) and acceptors (fullerenes) that were discussed in this review. Whereas, Table 1 lists all of the high-efficiency, 6 to 10 %, single-junction small molecule^{34,35,41} and polymer:fullerene^{1,19,20,27-29,42-48} solar cells that have been prepared through solution processing.

Controlling the microstructure of the active layer

Active layers with BHJ structures that consist of conjugated polymers as donors and nanometer-sized fullerenes as acceptors often form complicated morphologies that typically arise from limited polymer:fullerene miscibility, resulting in phase-separated polymer- and fullerene-rich domains that coexist with molecularly-mixed amorphous domains. An active layer incorporating phase-separated domains in a BHJ solar cell can affect the device performance because these domains provide not only interfaces for charge separation of photogenerated excitons but also percolation pathways for charge carrier transport to the respective electrodes; the former requires a fine dispersion of fullerene units in the polymer, due to the short exciton diffusion length in the polymer (≤ 10 nm), while the latter necessitates a decent fullerene domain size to form complementary interpenetrating networks for charge transport to the respective electrodes to avoid charge recombination⁴⁹. The morphology of the active layer can be controlled limitedly by varying parameters such as the chemical composition^{6,50-53}, the solvent used^{6,50}, and the postproduction treatment conditions^{51,52,54-61}, but often it is not understood *a priori*. It is, therefore, necessary to monitor the nanometer-scale domains of the active layer and correlate them with the device performance using various tools that can discriminate the small structure differences in polymer/fullerene composites processed using different solvents. X-ray and electron microscopy based techniques are widely utilized for characterizing the morphology of BHJ structures in reciprocal and real spaces, respectively. Grazing-incidence x-ray scattering is the most suitable method for obtaining statistically structural information from the square-millimeter area of a thin film, which is on the order of hundreds of nanometers thick^{27,51,53,61-67}. Probing the active layer through simultaneous grazing incidence wide- and small-angle x-ray scattering can provide global information regarding the polymer's crystallinity and internal structure of the dispersed fullerene units, allowing quantitative investigation of the mean size, volume fraction, and size distribution of the aggregated PCBM clusters⁶⁸. Kinetics studies⁶⁴ of fullerene aggregation and polymer crystallization have revealed that they often compete with each other, leading to quite different active layer microstructures for different material systems. Visualizing the cross-sectional morphologies of BHJ solar cells comprising structurally

(i) Donor: polymer



(ii) Acceptor: fullerene

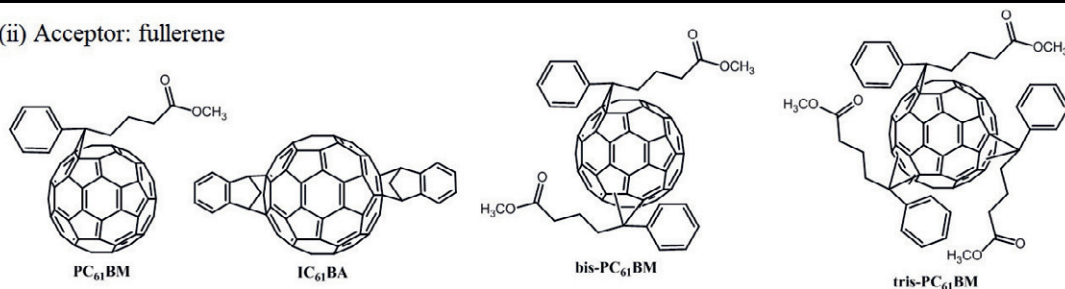


Fig. 4 Chemical structures of representative donors (polymers) and acceptors (fullerenes) discussed in this review article.

similar components, however, requires intricate characterization techniques, such as transmission electron microscopy (TEM)^{69–71}. In particular, recent works demonstrated that TEM tomography can be an effective way to characterize the three-dimensional morphology^{56,72} of OPVs. Fig. 5a presents the bright-field TEM image of an annealed regio-regular poly(3-hexyl thiophene) (P3HT):PC₆₁BM photoactive layer; the P3HT fibers and PCBM-rich domains are clearly discernable as bright and dark regions, respectively, because of their different densities (P3HT, 1.1 g/cm³; PC₆₁BM, 1.5 g/cm³). Fig. 5b shows a schematic drawing of a hierarchical P3HT:PC₆₁BM microstructure. In a pristine film, the fullerene moieties can disperse individually or form aggregated domains intercalated between P3HT lamellae and amorphous polymer chains. The sizes of the aggregated fullerene and P3HT lamellae domains show increasing after thermal annealing⁷³. Among the approaches developed for optimizing a BHJ device's active layer microstructure, the application of thermal and solvent annealing are the most common production ways to control the polymer:PC₆₁BM blend morphology. Recently, using solvent additive during processing of the active layer incorporating PC₇₁BM becomes the simplest and most effective way to optimize the

blend morphology; it influences the size of the fullerene domains and enhances the crystallinity of the self-organized polymers by improving the solubility of the fullerene moieties and slightly elongating the drying time of the active layer. The need exists for a solvent additive that can bridge the miscibility gap between the conjugated polymer and PC₇₁BM so that more-homogeneous films can be produced. Notably, the addition of DIO can significantly improve the miscibility of PC₇₁BM with the polymer. Moreover, the alkyl chain length of the additive can have a substantial effect on the morphology of the active layer and, therefore, the device's performance⁷⁴. The precise working mechanism behind the solvent additive's effect on the morphology of an active layer constituted by a crystalline polymer and a fullerene is not fully understood because of insufficient structural information extending from the nano- to the mesoscale.

Device structure and interfacial layer

At present, conventional and inverted device structures on indium tin oxide (ITO)-based electrode are two major configurations. The conventional configuration consists of glass/ITO/polyethylene

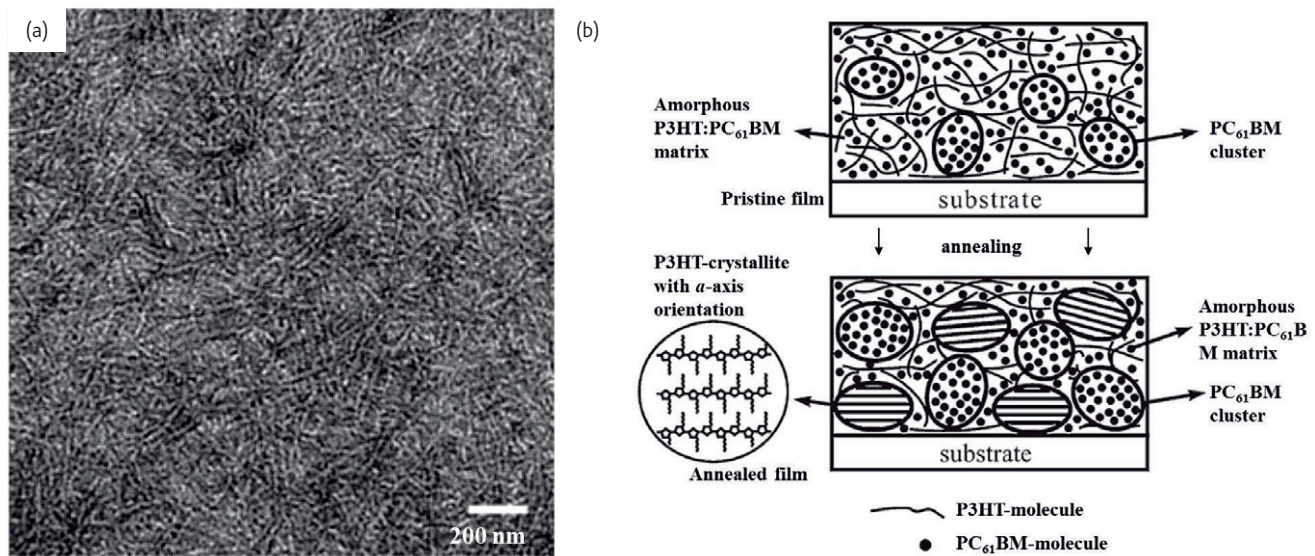


Fig. 5 (a) Bright-field TEM image of a thermally annealed P3HT:PCBM film. Reprinted with permission from Ref 56. Copyright © 2009 American Chemical Society) (b) Schematic drawings of the hierarchical structure in the nanometer-scale morphology in pristine and annealed P3HT:PCBM films. Reprinted with permission from Ref 73. Copyright © 2009 Wiley-VCH Verlag GmbH & Co.

Table 1. Device characterization data for single-junction small molecule or polymer with fullerene solar cells.

Small molecule: fullerene						
Ref.	Device configuration	Active area (cm ²)	V _{oc} (V)	J _{sc} (mA/cm ²)	FF	PCE (%)
^c Sun ³⁵	ITO/ MoO ₃ /DTS(PTTh ₂) ₂ :PC ₇₁ BM/Al	0.196	0.78	14.40	0.59	6.7
^c Zhou ³⁴	ITO/PEDOT:PSS/DCAO3TSi:PC ₆₁ BM/LiF/Al	0.04	0.80	11.51	0.64	5.8
^c Wei ⁴¹	ITO/ MoO ₃ /Squaraine:PC ₇₁ BM/C ₆₀ /BCP/Al	0.008	0.92	12.00	0.50	5.5
Polymer: fullerene						
Ref.	Device Configuration	active area (cm ²)	V _{oc} (V)	J _{sc} (mA/cm ²)	FF	PCE % *certified
Mitsubishi Chemical ¹	N/A	N/A	N/A	N/A	N/A	10.0*
ⁱ He ²⁹	ITO/PFN/PTB7:PC ₇₁ BM/ MoO ₃ /Al	0.16	0.75	17.46	0.70	9.2*
ⁱ Small ²⁸	ITO/ZnO-PVP/PDTS-TPD:PC ₇₁ BM/MoO ₃ /Ag	0.03	0.86	14.00	0.67	8.5 7.4*
^c Chen ¹⁹	ITO/PEDOT:PSS/PBDTTT-CF:PC ₇₁ BM/Ca/Al	0.1	0.75	15.20	0.67	7.7 6.8*
ⁱ Tan ⁴²	ITO/TiPD/PBDTTT-C:PC ₇₁ BM/MoO ₃ /Ag	0.04	0.70	16.26	0.65	7.4
ⁱ You ⁴³	ITO/ZnO/PTB7:PC ₇₁ BM/MoO ₃ /Ag	0.1	0.72	14.72	0.69	7.3
^c Su ²⁷	ITO/PEDOT:PSS/PBTPDP:PC ₇₁ BM/Ca/Al	0.04	0.92	13.10	0.61	7.3
^c Zhou ²⁰	ITO/PEDOT:PSS/PBnDT-DTffBT:PC ₆₁ BM/Ca/Al	0.12	0.91	12.91	0.61	7.2
ⁱ Chang ⁴⁴	ITO/ZnO/C-PCBSD/PFDCTBT-C8:PC ₇₁ BM/PEDOT:PSS/VO ₂ /Ag	0.04	0.83	12.57	0.67	7.0
ⁱ Chu ⁴⁵	ITO/ZnO/PDTSTPD:PC ₇₁ BM/MoO ₃ /Ag	1.0	0.89	11.30	0.67	6.7
^c Fan ⁴⁶	ITO/MoO ₃ /P3HT:IC ₇₀ BA/Ca/Al	0.04	0.85	10.61	0.74	6.7
^c Zhang ⁴⁷	ITO/PEDOT:PSS/PIDT-phanQ:PC ₇₁ BM/C ₄ /Al	0.1	0.87	11.20	0.64	6.2
^c O'Malley ⁴⁸	ITO/PEDOT:PSS/PIDT-phanQ:PC ₇₁ BM/C ₆₀ -bis/Ag	0.046	0.88	11.50	0.61	6.2

ⁱ: Inverted structure
^c: Conventional structure

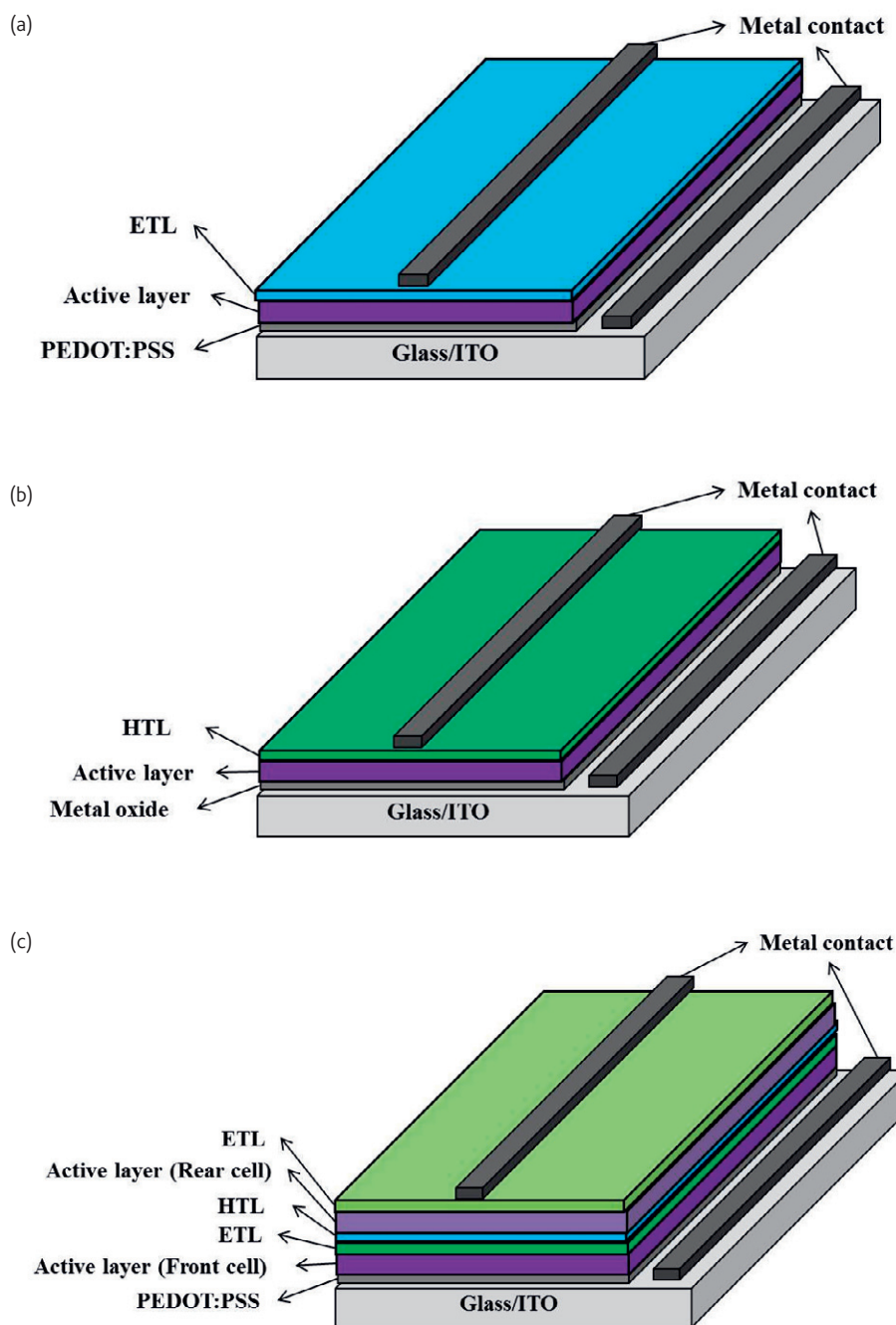


Fig. 6 Device structures of (a) conventional single-junction cell, (b) inverted single-junction cell, and (c) conventional multi-junction tandem cells.

dioxythiophene:polystyrene sulfonate (PEDOT:PSS)/active layer/cathode interlayer (e.g., Ca or LiF/Al). Oxidation of the low-work-function electrode (e.g., Al) can make the device unstable in air; therefore, more sophisticated encapsulation techniques may be necessary. The inverted configuration comprises glass/ITO/metal oxide/active layer/interfacial layer/Ag; where Ag with its high work function is introduced as the top electrode, and an oxide interfacial layer is introduced between the active

layer and the top cathode. To fulfill the goal of using solution processing in each step, zinc oxide (ZnO) nanoparticle⁷⁵⁻⁷⁸ interfacial layer was spin-coated because of its relative high electron mobility. Figure 6(a) and (b) display the conventional and inverted organic solar cells, respectively. In theory, the PCE of a single-junction cell can be pushed toward 15 %⁷⁹ if low-bandgap polymers are introduced. Optical simulation⁸⁰ data have revealed that the value of J_{sc} of an inverted device could be greater

Table 2. Device characterization data for multi-junction polymer solar cells.

Ref.	Device configuration	Active area (cm ²)	V _{oc} (V)	J _{sc} (mA/cm ²)	FF	PCE % *certified
UCLA-Sumitomo ¹	N/A	N/A	1.50	8.75	N/A	10.6*
[†] Dou ¹⁸	ITO/ZnO/P3HT:IC ₆₀ BA/PEDOT:PSS/ZnO/PBDTT-DPP:PC ₇₁ BM/MoO ₃ /Ag	0.1	1.56	8.26	0.67	8.6*
[†] Yang ⁸³	ITO/Ag/P3HT:IC ₆₀ BA/TiO ₂ /m-PEDOT/PSBTBT:PC ₇₁ BM/V ₂ O ₅ /Al	N/A	1.47	7.60	0.63	7.0
[†] Gevaerts ⁸⁴	ITO/PEDOT:PSS/PCDTBT:PC ₇₁ BM/ZnO/PEDOT:PSS/PDPP5T:PC ₆₁ BM/Al	0.16	1.44	9.00	0.54	7.0
[†] Kim ⁸⁵	ITO/PEDOT:PSS/PCPDTBT:PC ₆₁ BM/TiO _x /PEDOT:PSS/P3HT:PC ₇₁ BM/TiO _x /Al	0.045	1.24	7.80	0.67	6.5
[†] Sista ⁸⁶	ITO/PEDOT:PSS/P3HT:PC ₇₁ BM/Al/TiO ₂ /PEDOT:PSS/PSBTBT:PC ₇₁ BM/TiO ₂ :Cs/Al	N/A	1.25	7.44	0.63	5.8
[†] Kouijzer ⁸⁷	ITO/ZnO/P3HT:IC ₆₀ BA/PEDOT:PSS/ZnO/PDPP5T:PC ₆₁ BM/MoO ₃ /Ag	0.16	1.35	7.23	0.60	5.8
[†] Kong ⁸⁸	ITO/PEDOT:PSS/SDT-BT:PC ₇₁ BM/TiO _x /PEDOT:PSS/P3HT:PC ₇₁ BM/TiO _x /Al	0.14	1.17	7.20	0.62	5.2
[†] Sakai ⁸⁹	ITO/PEDOT:PSS/P3HT:bis-PC ₆₁ BM/LiF/ITO/MoO ₃ /P3HT:PC ₇₁ BM/LiF/Al	0.06	1.14	6.14	0.74	5.2
[†] Chou ⁹⁰	ITO/ZnO/P3HT:PC ₆₁ BM/MoO ₃ /Al/ZnO/PSBTBT:PC ₇₁ BM/MoO ₃ /Al	0.093	1.20	7.84	0.54	5.1

[†]: Inverted structure
[†]: Conventional structure

than that of a normal device, but the values of V_{oc}, FF, and PCE would be lower. To overcome this limitation, the concept of multi-junction (tandem) cells⁸¹ was proposed to increase values of V_{oc}. Fig. 6(c) presents a schematic representation of a multi-junction tandem cell having the conventional configuration. Two sub-cells are stacked and separated by the electron-transporting layer (ETL) and the hole-transporting layer (HTL), which can collect electrons from the front cell and holes from the rear cell, respectively. The V_{oc} of a multi-junction cell can be estimated by summing the V_{oc} of the front and rear cells. To broaden the light absorption range, a low-bandgap polymer was employed for the rear cell to absorb the residual light from the front cell⁸². Table 2 lists all of the high-efficiency, 5 to 10.6 %, multi-junction polymer:fullerene solar cells that include conventional and inverted device structures^{18,83-90}. An efficiency of 10.6 %, the highest PCE, for a multi-junction OPV that was developed by UCLA and Sumitomo Chemical Corporation jointly has been posted on the NREL website without detailing its active layer or device structures. For all OPVs, the active area of the devices that had been used was between 0.04 and 1 cm² as shown in Table 1 and 2. The FF and therefore the PCE, however, were found to decrease with the increasing active area of the OPVs⁹¹.


In addition to the ITO-based electrode, there are other types of electrodes such as silver nanowires⁹², modified PEDOT:PSS layer^{93,94} and graphene⁹⁵ that have been developed for OPVs. The ultimate goal of the development of electrodes is to have solution-processable transparent electrodes that have similar electrical resistance to that of ITO and are compatible with the roll-to-roll fabrication techniques. Last and equally important, the stability of OPVs is a main concern and can be the largest

hurdle for their future commercialization. The stability of OPVs can now exceed many thousands hours⁹⁶ with only slight decay in the PCE. This progress has been attributed to several developments such as inverted device structures that allows for more stable metal electrodes, the choice of crystalline active materials and the introduction of interfacial materials, and more efforts should be carried out in these regards in the near future.

Conclusion and future prospects

The great progress in OPVs in the last ten years can be attributed to advances in four fronts: (i) a better understanding of the fundamental mechanism of photon-to-electron conversion; (ii) advances in the molecular design of new materials with tailored energy levels and solubility; (iii) new processing approaches to induce the optimal microstructure in the active layer and new progress in the application of analytical tools; and (iv) new device architectures with developments in optimizing the interfacial layers. To reach the "holy grail" of high-PCE OPVs (cell: >15 %; module: >10 %) having large areas, fabricated through roll-to-roll solution processes, and exhibiting device life times of greater than ten years will, however, require concerted interdisciplinary efforts by both scientists and engineers to provide new approaches toward solving critical technical issues. For instance, scientists must be able to prepare multifunctional organic molecular structures that absorb into the visible and IR regions while exhibiting good photo-stability, to synthesize new fullerene structures displaying complementary absorptions and good solubility, and to perform simulations on material properties with different chemical units; they also must have the ability to develop

approximate physical device frameworks for simulations and to design the optimal active layer microstructure. Engineers must devise suitable scale-up roll-to-roll fabrication processes and packaging for OPVs incorporating various materials, design different types of electrodes

that can be solution-processed and minimize the gap between the PCEs of cells and modules and enhance the stability of OPVs. With these combined efforts, it is likely that the commercialization of OPVs will be realized within a few years. 

References

- NREL, In <http://www.nrel.gov/ncpv/>
- Forrest, S. R., *Nature* (2004) **428** (6986), 911
- Deibel, C., and Dyakonov, V., *Rep Prog Phys* (2010) **73** (9), 096401
- Peumans, P., et al., *J Appl Phys* (2003) **93** (7), 3693
- Brabec, C. J., et al., *Chem Phys Lett* (2001) **340** (3-4), 232
- Park, S. H., et al., *Nat Photonics* (2009) **3** (5), 297
- Mayer, A. C., et al., *Adv Funct Mater* (2009) **19** (8), 1173
- Bredas, J. L., et al., *Chem Rev* (2004) **104** (11), 4971
- Yu, G., and Heeger, A. J., *J Appl Phys* (1995) **78** (7), 4510
- Gunes, S., et al., *Chem Rev* (2007) **107** (4), 1324
- Roncali, J., *Chem Rev* (1997) **97** (1), 173
- Mcculloch, I., et al., *Accounts Chem Res* (2012) **45** (5), 714
- Zhou, H. X., et al., *Macromolecules* (2012) **45** (2), 607
- Zhou, H. X., et al., *Macromolecules* (2010) **43** (24), 10390
- Chen, H. Y., et al., *Adv Mater* (2010) **22** (3), 371
- Jiang, J. M., et al., *Chem Commun* (2011) **47** (31), 8877
- Huo, L. J., et al., *Angew Chem Int Edit* (2010) **49** (8), 1500
- Dou, L. T., et al., *Nat Photonics* (2012) **6** (3), 180
- Chen, H. Y., et al., *Nat Photonics* (2009) **3** (11), 649
- Zhou, H. X., et al., *Angew Chem Int Edit* (2011) **50** (13), 2995
- Piliago, C., et al., *J Am Chem Soc* (2010) **132** (22), 7595
- Chen, G. Y., et al., *Chem Commun* (2011) **47** (17), 5064
- Ottone, C., et al., *Polym Chem-Uk* (2012) **3** (9), 2355
- Chu, T. Y., et al., *J Am Chem Soc* (2011) **133** (12), 4250
- Amb, C. M., et al., *J Am Chem Soc* (2011) **133** (26), 10062
- Yuan, M. C., et al., *Macromolecules* (2010) **43** (17), 6936
- Su, M. S., et al., *Adv Mater* (2011) **23** (29), 3315
- Small, C. E., et al., *Nat Photonics* (2012) **6** (2), 115
- He, Z. C., et al., *Nat Photonics* (2012) **6** (9), 591
- Chang, Y. T., et al., *Adv Mater* (2009) **21** (20), 2093
- Huang, F., et al., *J Am Chem Soc* (2009) **131** (39), 13886
- Duan, C. H., et al., *Chem Mater* (2010) **22** (23), 6444
- Zhang, Z. G., et al., *Macromolecules* (2012) **45** (5), 2312
- Zhou, J. Y., et al., *Chem Mater* (2011) **23** (21), 4666
- Sun, Y. M., et al., *Nat Mater* (2012) **11** (1), 44
- Azimi, H., et al., *Adv Energy Mater* (2011) **1** (6), 1162
- Guilbert, A. A. Y., et al., *Acs Nano* (2012) **6** (5), 3868
- He, Y. J., et al., *J Am Chem Soc* (2010) **132** (4), 1377
- He, Y. J., et al., *Adv Funct Mater* (2010) **20** (19), 3383
- Zhao, G. J., et al., *Adv Mater* (2010) **22** (39), 4355
- Wei, G. D., et al., *Adv Energy Mater* (2011) **1** (2), 184
- Tan, Z. A., et al., *Adv Mater* (2012) **24** (11), 1476
- You, J., et al., *Adv Mater* (2012) **24** (38), 5267
- Chang, C. Y., et al., *Adv Mater* (2012) **24** (4), 549
- Chu, T. Y., et al., *Sol Energy Mat Sol C* (2012) **96** (1), 155
- Fan, X., et al., *Adv Funct Mater* (2012) **22** (3), 585
- Zhang, Y., et al., *Chem Mater* (2011) **23** (9), 2289
- O'Malley, K. M., et al., *Adv Energy Mater* (2012) **2** (1), 82
- Nelson, J., et al., *Accounts Chem Res* (2009) **42** (11), 1768
- Barrau, S., et al., *Macromolecules* (2009) **42** (13), 4646
- Li, G., et al., *Adv Funct Mater* (2007) **17** (10), 1636
- Xin, H., et al., *Acs Nano* (2010) **4** (4), 1861
- Chiu, M. Y., et al., *Macromolecules* (2010) **43** (1), 428
- Padinger, F., et al., *Adv Funct Mater* (2003) **13** (1), 85
- Stevens, D. M., et al., *J Phys Chem C* (2009) **113** (26), 11408
- van Bavel, S. S., et al., *Nano Lett* (2009) **9** (2), 507
- Honda, S., et al., *Acs Appl Mater Inter* (2009) **1** (4), 804
- Tsoi, W. C., et al., *Macromolecules* (2011) **44** (8), 2944
- Kozub, D. R., et al., *Macromolecules* (2011) **44** (14), 5722
- Chen, D. A., et al., *Nano Lett* (2011) **11** (2), 561
- Chen, D., et al., *Nano Lett* (2011) **11** (5), 2071
- Lilliu, S., et al., *Macromolecules* (2011) **44** (8), 2725
- Yin, W., and Dadmun, M., *Acs Nano* (2011) **5** (6), 4756
- Wu, W. R., et al., *Acs Nano* (2011) **5** (8), 6233
- Chiu, M. Y., et al., *Adv Mater* (2008) **20** (13), 2573
- Chen, H. Y., et al., *J Phys Chem C* (2009) **113** (18), 7946
- Sirringhaus, H., et al., *Nature* (1999) **401** (6754), 685
- Liao, H. C., et al., *J Am Chem Soc* (2011) **133** (33), 13064
- Moon, J. S., et al., *Nano Lett* (2009) **9** (1), 230
- Moon, J. S., et al., *Nano Lett* (2011) **11** (3), 1036
- Pfannmoller, M., et al., *Nano Lett* (2011) **11** (8), 3099
- van Bavel, S. S., et al., *Adv Funct Mater* (2010) **20** (9), 1458
- Dennler, G., et al., *Adv Mater* (2009) **21** (13), 1323
- Lee, J. K., et al., *J Am Chem Soc* (2008) **130** (11), 3619
- White, M. S., et al., *Appl Phys Lett* (2006) **89** (14)
- Hau, S. K., et al., *Appl Phys Lett* (2008) **92** (25)
- Stubhan, T., et al., *Org Electron* (2011) **12** (9), 1539
- Sun, Y. M., et al., *Adv Mater* (2011) **23** (14), 1679
- Dennler, G., et al., *Adv Mater* (2008) **20** (3), 579
- Albrecht, S., et al., *Org Electron* (2012) **13** (4), 615
- Gilot, J., et al., *Appl Phys Lett* (2007) **90** (14)
- Hadipour, A., et al., *Adv Funct Mater* (2008) **18** (2), 169
- Yang, J., et al., *Adv Mater* (2011) **23** (30), 3465
- Gevaerts, V. S., et al., *Adv Mater* (2012) **24** (16), 2130
- Kim, J. Y., et al., *Science* (2007) **317** (5835), 222
- Sista, S., et al., *Adv Mater* (2010) **22** (3), 380
- Kouijzer, S., et al., *Adv Energy Mater* (2012) **2** (8), 945
- Kong, J., et al., *Phys Chem Chem Phys* (2012) **14** (30), 10547
- Sakai, J., et al., *Sol Energy Mat Sol C* (2010) **94** (2), 376
- Chou, C. H., et al., *Adv Mater* (2011) **23** (10), 1282
- Manor, A., et al., *J Appl Phys* (2011) **109** (7), 074508
- Chen, C. C., et al., *Acs Nano* (2012) **6** (8), 7185
- Kim, Y. H., et al., *Adv Funct Mater* (2011) **21** (6), 1076
- Alemu, D., et al., *Energ Environ Sci* (2012) **5** (11), 9662
- Hsu, C. L., et al., *Acs Nano* (2012) **6** (6), 5031
- Jorgensen, M., et al., *Adv Mater* (2012) **24** (5), 580